Chemical Science

ROYAL SOCIETY OF CHEMISTRY

EDGE ARTICLE

View Article Online
View Journal | View Issue

Cite this: *Chem. Sci.*, 2024, **15**, 13234

All publication charges for this article have been paid for by the Royal Society of Chemistry

Received 30th March 2024
Accepted 29th June 2024

DOI: 10.1039/d4sc02103g

rsc.li/chemical-science

Helicity control of a polyaromatic coordination capsule through stereoselective CH–π interactions†

Natsuki Kishida, Hayate Sasafuchi, Tomohisa Sawada and Michito Yoshizawa *

Although square-planar ML_4 units are essential building blocks for coordination cages and capsules, the non-covalent control of the chirality and helicity of the resultant nanostructures is quite difficult. Here we report the helicity control of an M_2L_4 polyaromatic capsule, formed from metal ions with square-planar coordination geometry and bent bispyridine ligands, through stereoselective CH–π interactions with monosaccharide derivatives. Thanks to host–guest CH–π multi-interactions, one molecule of various permethylated monosaccharides is quantitatively bound by the capsule in water (K_a up to $>10^8$ M^{-1}). In the polyaromatic cavity, among them, the selective binding of a β-glucose derivative (>80 : 20 ratio) is demonstrated from a mixture of the α/β-glucoses, through the *equatorial*-selective recognition of the anomeric (C1) group. A similar stereoselective binding is accomplished from an α/β-galactose mixture. Interestingly, single equatorial/axial configurations on the bound monosaccharides can regulate the helical conformation of the capsule in water, confirmed by CD, NMR, and theoretical analyses. An intense capsule-based Cotton effect is exclusively observed upon encapsulation of the permethylated α-glucose (>20-fold enhancement as compared to the β-glucose derivative), *via* the induction of a single-handed host helicity to a large extent. Inverse capsule helicity is induced by the binding of a β-galactose derivative under the same conditions.

Introduction

Precise control of the chirality and helicity of supramolecular architectures is receiving increasing attention from the viewpoints of chiroptical synthetic, materials, and analytical chemistry.[1,2] Square-planar ML_4 units (M = metal ion, L = monodentate ligand) are indispensable building blocks for the design and creation of supramolecular cages and capsules.[3] The $M(pyridyl)_4$ unit (Fig. 1a) has been predominantly employed among them, due to suitable binding strength and stability.[3–5] Whereas the metal hinge can adopt propeller-like helical conformations, the right- and left-handed forms are in rapid equilibrium in solution (Fig. 1b), in marked contrast to Δ/Λ octahedral ML'_3 units (L′ = bidentate chelating ligand; Fig. 1c) as non-equilibrium chiral building blocks.[6] Therefore, the majority of square-planar metal hinge-based M_nL_m cages and capsules are obtained as racemic mixtures in solution.[7] Their racemization has been exceptionally regulated by covalently embedding chiral or helical units into the host frameworks.[8] However, non-covalent interactions, *e.g.*, *via* solvent/temperature change, counter ion exchange, and guest addition, are typically ineffective for the

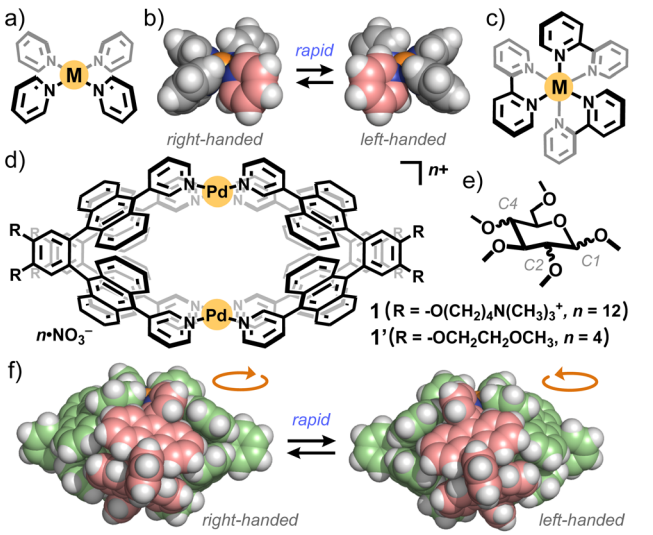

Fig. 1 (a) Representative square-planar ML_4 unit and (b) its right/left-handed forms. (c) Representative octahedral ML'_3 unit as a chiral building block. (d) Polyaromatic coordination capsule **1** with ionic side chains (this work) and its analogue **1′** (previous work). (e) Permethylated monosaccharides as water-soluble chiral guests. (f) Right/left-handed helical frameworks of **1′** (R = H for clarity).[13b]

Laboratory for Chemistry and Life Science, Institute of Innovative Research, Tokyo Institute of Technology, 4259 Nagatsuta, Midori-ku, Yokohama 226-8503, Japan. E-mail: yoshizawa.m.ac@m.titech.ac.jp

† Electronic supplementary information (ESI) available. See DOI: https://doi.org/10.1039/d4sc02103g

regulation of such racemic nanostructures,[9] owing to the low inversion energies of the square-planar metal sites.

Here we realize the helicity control of M_2L_4 polyaromatic capsule **1** (Fig. 1d) through non-covalent, stereoselective CH–π multi-interactions with monosaccharide derivatives in water. The coordination capsule provides right- and left-handed helical structures, based on the square-planar metal hinges, as a racemic mixture (Fig. 1f). For the regulation of the capsule helicity, permethylated monosaccharides (Fig. 1e) are employed as chiral guests to maximize host–guest CH–π interactions in the spheroidal polyaromatic cavity. Monosaccharides are ubiquitous biosubstrates with equatorial/axial hydroxy groups.[10] Their permethylated derivatives,[11] facilely accessed from natural saccharides, are thus suitable guests to study stereoselective CH–π recognition and interactions.[12] Using water-soluble capsule **1** (Fig. 1d), we herein report the selective binding of a β-glucose derivative (81 : 19 ratio) from a mixture of α/β-glucoses in water, through the *equatorial* recognition of a methoxy group on the anomeric (C1) position. A similar stereoselective binding is accomplished from an α/β-galactose mixture. The C4 and C2 groups are also recognized by the capsule, from mixtures of β-glucose/β-galactose and α-glucose/α-mannose derivatives, respectively, with high equatorial selectivity (up to 89 : 11 ratio). Notably, only single equatorial/axial configurations on the monosaccharides can control the right- and left-handed conformations of the capsule, *via* the efficient guest-induced helicity control of the host framework, which are revealed by the combination of circular dichroism (CD), NMR, and theoretical studies.

A spheroidal polyaromatic cavity (1.0 × 1.5 × 1.5 nm^3) is provided by coordination capsule **1′** (Fig. 1d), formed by the quantitative assembly from two Pd(II) ions with square-planar coordination geometry and four bispyridine ligands, bearing two anthracene panels linked by an *ortho*-phenylene spacer.[13a] The capsule framework, which is a tightly wound polyaromatic shell, adopts right- and left-handed twist forms in a 1 : 1 ratio, with partially overlapped anthracene units (Fig. 1f). In the polyaromatic cavity, one molecule of planar and bowl-shaped aromatic molecules (*e.g.*, coronene and sumanene) are efficiently encapsulated through multiple *aromatic* CH–π interactions in organic solvents.[13b] The shape of the aromatic molecules is selectively recognized through the number of the host–guest interactions in the racemic cavity.[13c] To facilitate *aliphatic* CH–π interactions with bio-related substrates, we designed analogous capsule **1** with water solubility (Fig. 1d), featuring eight ionic side chains on the polyaromatic shell. Monosaccharides, focused in this study, adopt multiple stereoisomers derived from the five equatorial/axial substituents on the six-membered ring. Whereas monomethylated β-glucose can be favourably bound over its α-isomer by synthetic covalent cages,[14] the equatorial/axial-selective binding of oligomethylated glucose and other saccharides remains to be accomplished so far.[3,15]

Results and discussion

Preparation of a water-soluble polyaromatic capsule

To study host–guest interactions under aqueous conditions, polyaromatic capsule **1** was prepared from $Pd(NO_3)_2$ and

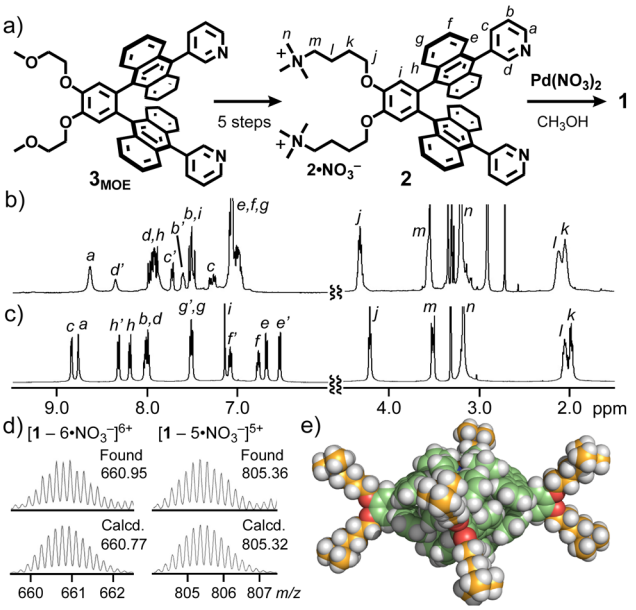

Fig. 2 (a) Synthesis of cationic ligand **2** and the formation of water-soluble polyaromatic capsule **1** as a racemic mixture. ^{1}H MNR spectra (500 MHz, CD_3OD, r.t.) of (b) **2** and (c) **1**. (d) ESI-TOF MS spectra (CH_3OH) of **1** and the calculated isotope patterns. (e) Optimized structure of **1** (DFT calculation, CAM-B3LYP/3-21G).

dicationic ligand **2**, through the simple attachment of pendant trimethylammonium groups on bent bispyridine ligand $\mathbf{3_{MOE}}$ (Fig. 2a and S1–14†).[16,17] The quantitative formation of the new coordination capsule, with an M_2L_4 composition, was confirmed by NMR and MS analyses (Fig. S15–18†).[16,17] In the ^{1}H NMR spectra, although ligand **2** showed complicated signals derived from the rotational isomers based on the pyridyl groups, capsule **1** provided highly symmetrical signals with 13 aromatic signals ($H_{a–i}$, 8.8–6.5 ppm) and 5 aliphatic signals ($H_{j–n}$, 4.2–2.0 ppm; Fig. 2b and c). The desymmetrisation of the anthracene-based signals ($H_{e,e',f,f',g,g',h,h'}$) suggested the existence of right- and left-handed helical capsules, owing to the partial anthracene stacks. The ESI-TOF MS spectrum of **1** showed molecular ion peaks at m/z = 557.53, 660.95, 805.36, and 1022.42, assignable to $[\mathbf{1} - n \cdot NO_3^-]^{n+}$ ions (n = 7–4; Fig. 2d and S18†). In the optimized structure of **1**, the helical, hydrophobic capsular flamework is surrounded by eight hydrophilic groups (Fig. 2e). Whereas previous capsule **1′** is insoluble in water even at elevated temperature,[13b] the present one showed adequate water solubility (>10 mM) at room temperature.

Equatorial-selective binding of monosaccharides in water

The equatorial and axial configuration on D-glucose derivatives could be selectively distinguished by polyaromatic capsule **1** through competitive binding experiments in water. When a mixture of hydrophilic permethylated α-D-glucose ($\mathbf{\alpha Glc^{Me}}$) and β-D-glucose ($\mathbf{\beta Glc^{Me}}$; 0.20 μmol each) was combined with capsule **1** (0.10 μmol) in D_2O (0.5 mL) at 80 °C for 10 min, 1 : 1 host–guest complexes $\mathbf{1 \cdot \alpha Glc^{Me}}$ and $\mathbf{1 \cdot \beta Glc^{Me}}$ were formed in 19 and 81% yields based on **1**, respectively (Fig. 3a). In the ^{1}H NMR spectra, the multiple aromatic signals of empty **1** (8.9–6.6 ppm) were fully

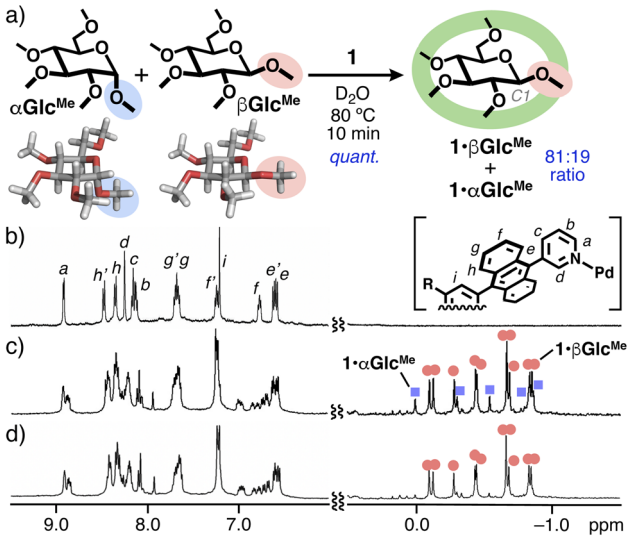

Fig. 3 (a) Selective binding of **βGlc^{Me}** by capsule **1** in water from a 1 : 1 mixture of **αGlc^{Me}** and **βGlc^{Me}**. ^{1}H NMR spectra (500 MHz, D_2O, r.t.) of (b) **1**, (c) the resultant host–guest complexes obtained from a mixture of **1**, **αGlc^{Me}**, and **βGlc^{Me}**, and (d) **1·βGlc^{Me}**.

converted to those of the new host–guest complexes (Fig. 3b and c, left), suggesting the quantitative binding of the water-soluble substrates. The complete encapsulation of the substrates was indicated by the appearance of all the methyl groups on **αGlc^{Me}** (five signals) and **βGlc^{Me}** (ten signals) in the range of 0.00 to −0.87 ppm (Fig. 3b and c, right). The remarkable upfield shifts ($\Delta\delta_{max} = -4.4$ ppm) of the signals, relative to those of the free substrates in D_2O (3.6–3.4 ppm), are derived from the strong shielding effect in the polyaromatic cavity of **1**. On the basis of the methyl signals of **1·αGlc^{Me}** and **1·βGlc^{Me}**, prepared separately from **1** and **αGlc^{Me}** or **βGlc^{Me}** (Fig. 3d and S19–20†), the selective formation of **1·βGlc^{Me}** (81 : 19 ratio) was readily estimated by their non-overlapping signal integrals (Fig. S28c†).[16] The result revealed that the anomeric (C1) group on the monosaccharides is equatorial-selectively recognized by the present capsule through spheroidal cavity-directed host–guest interactions. The quantitative binding was also performed even at 40 °C for 2 h, with a similar equatorial-selectivity (*i.e.*, an 82 : 18 ratio; Fig. S28d†).[16] The selectivity coefficient value (K(**βGlc^{Me}**)/K(**αGlc^{Me}**)) of **1** was calculated to be 6.5.

Similar equatorial-selective interactions were observed between α-D-galactose (**αGal^{Me}**) and β-D-galactose derivatives (**βGal^{Me}**) as well as **βGlc^{Me}** and **βGal^{Me}** within the polyaromatic capsule. Under the same conditions of the competitive binding study with **α/βGlc^{Me}**, the treatment of a 1 : 1 mixture of **αGal^{Me}** and **βGal^{Me}** with **1** in D_2O led to the formation of host–guest complexes **1·βGal^{Me}** and **1·αGal^{Me}** in an 86 : 14 ratio (Fig. 4a), owing to the recognition of the C1 group. Methyl proton signals derived from **1·βGal^{Me}** and **1·αGal^{Me}** were again observed in the highly upfield region (from 0.31 to −1.2 ppm; Fig. 4f and S29†). Notably, further high equatorial-preference was demonstrated from a mixture of **βGlc^{Me}** and **βGal^{Me}** under the same conditions. The unusual recognition of the C4 group allowed **1** to generate **1·βGlc^{Me}** and **1·βGal^{Me}** in an 89 : 11 ratio (Fig. 4b, g

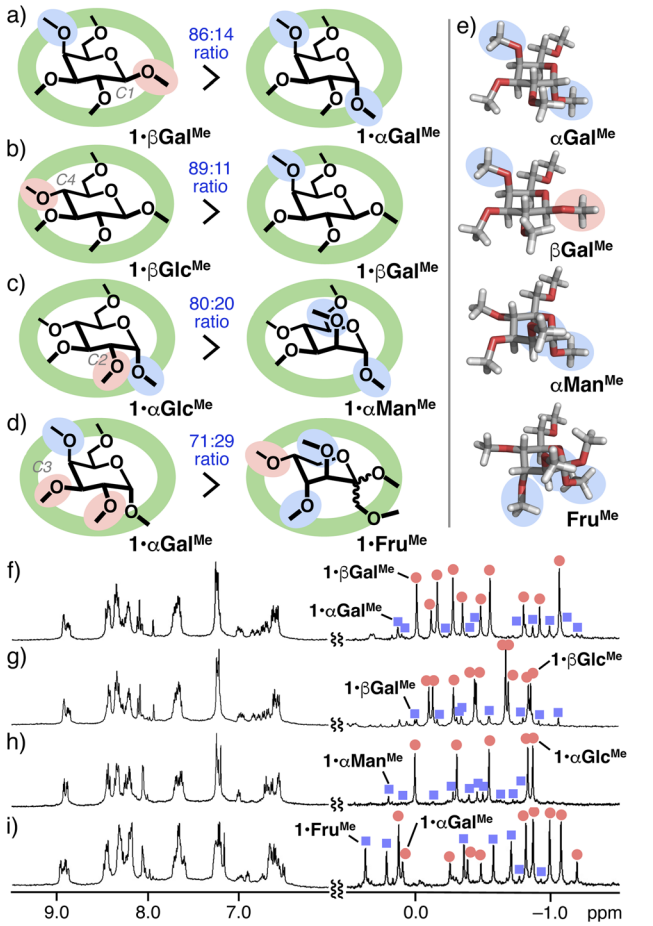

Fig. 4 Selective binding abilities of capsule **1** toward (a) **βGal^{Me}** from a mixture of **βGal^{Me}** and **αGal^{Me}**, (b) **βGlc^{Me}** from a mixture of **βGlc^{Me}** and **βGal^{Me}**, (c) **αGlc^{Me}** from a mixture of **αGlc^{Me}** and **αMan^{Me}**, and (d) **αGal^{Me}** from a mixture of **αGal^{Me}** and **Fru^{Me}** in water. (e) Optimized structures of **αGal^{Me}**, **βGal^{Me}**, **αMan^{Me}**, and **Fru^{Me}** (DFT calculation, B3LYP/6-31G(d,p)). ^{1}H NMR spectra (500 MHz, D_2O, r.t.) of host–guest complexes obtained from mixtures of (f) **βGal^{Me}** and **αGal^{Me}**, (g) **βGlc^{Me}** and **βGal^{Me}**, (h) **αGlc^{Me}** and **αMan^{Me}**, and (i) **αGal^{Me}** and **Fru^{Me}** with **1** in water after 10 min at 80 °C.

and S30†).[18] Equatorial-selectivity for the C2 group was also found within **1** for an **αGlc^{Me}** and α-D-mannose (**αMan^{Me}**) mixture (Fig. 4c, h, and S31†).[16] Capsule **1** bound **αGal^{Me}** over mixed α/β-D-fructopyranoses (**α/βFru^{Me}**), bearing three axial groups, in a 71 : 29 ratio under the same conditions (Fig. 4d, i, and S35†). Notably, the observed high selectivity toward **βGlc^{Me}** was also supported by a dilution experiment of **1·βGlc^{Me}** with water, where the binding constant (K_a) was roughly estimated to $>10^8$ M^{-1} (Fig. S27†).[16] The preferential binding ability of the capsule toward **βGlc^{Me}** over **αGlc^{Me}** and the other tested substrates is most probably derived from the shape fitting between the spheroidal host cavity and the comparatively planar guest structure (Fig. 3a and 4e).

Multiple CH–π interactions in the polyaromatic cavity

To understand the observed quantitative binding of the monosaccharide derivatives with unusually high equatorial-

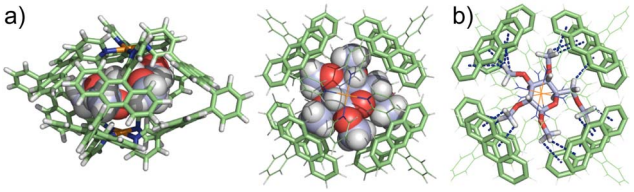

Fig. 5 (a) Optimized structure of (*P*)-**1**·**βGlc**^{Me} (side and top views; R = H for clarity) and (b) the highlighted guest (methyl groups)-host (anthracene panels) CH–π interactions in the cavity as blue dashed lines (distance: ≤3.6 Å).

selectivity, host–guest interactions within polyaromatic capsule **1** were quantified by DFT calculations.[19] In the optimized structure of **1**·**βGlc**^{Me}, the planar framework of **βGlc**^{Me} is fully accommodated in the spheroidal cavity of **1** and surrounded by multiple polyaromatic panels (Fig. 5a). The five methyl groups of bound **βGlc**^{Me} are located close to the eight anthracene rings of **1**, with contact distances of ≤3.6 Å (Fig. 5b).[19] On the basis of the distances, the presence of 19 CH–π interactions was indicated in the polyaromatic cavity. The optimized structure of **1**·**αGlc**^{Me}, with a slightly hindered axial-methoxy group, also suggested the existence of multiple CH–π interactions (Fig. S37†). The close contacts between the host frameworks (*e.g.*, $H_{d,e,f}$) and the guest methyl groups (*e.g.*, $H_{C,D}$) in the cavity were supported by the NOESY studies of **1**·**αGlc**^{Me} (Fig. S19c†). These host–guest contacts are consistent with the huge upfield shifts of the methyl signals of **βGlc**^{Me} and **αGlc**^{Me} within **1** in the ^{1}H NMR spectra (Fig. 3c).

Helicity control through stereoselective host–guest interactions

Notably, unlike previously reported coordination cages with square-planar metal hinges,[4,5,7–9] the right/left-handed twists of the present capsule (*i.e.*, (*P*)/(*M*)-helical structures) could be exclusively controlled through encapsulation of permethylated α-glucose **αGlc**^{Me}, which was confirmed by CD, NMR, and theoretical analyses. The UV-visible spectra of **1**, **1**·**αGlc**^{Me}, and **1**·**βGlc**^{Me} in water showed comparable absorption bands in the range of 320 to 450 nm (Fig. 6a), derived from the anthracene-based framework of the capsule. In the CD spectra in the range of 300–500 nm, whereas no signal was detected from both empty capsule **1** and free **α**/**βGlc**^{Me}, prominent CD signals, with a negative peak at 421 nm and positive peaks at 406, 387, 368 and 330 nm, were observed from host–guest complex **1**·**αGlc**^{Me} (Fig. 6b). The observed, relatively strong Cotton effect in the UV-visible region (θ_{max} = +79.5, λ = 387 nm) is attributed to the helical host framework of **1**, induced by binding of the chiral guest in the cavity. In sharp contrast, a relatively weak Cotton effect (θ_{max} = +3.3, λ = 387 nm) was observed in the CD spectrum of **1**·**βGlc**^{Me} under the same conditions. The maximum peak intensity of **1**·**αGlc**^{Me} is >20-fold higher than that of **1**·**βGlc**^{Me}. Therefore, the equatorial or axial configuration on the single glucose C1 group largely controlled the helicity of the capsular polyaromatic framework. The CD studies of host–guest complexes **1**·**α**/**βGal**^{Me} also revealed the helicity switch of the capsule using galactoses **αGal**^{Me} and **βGal**^{Me}. Interestingly,

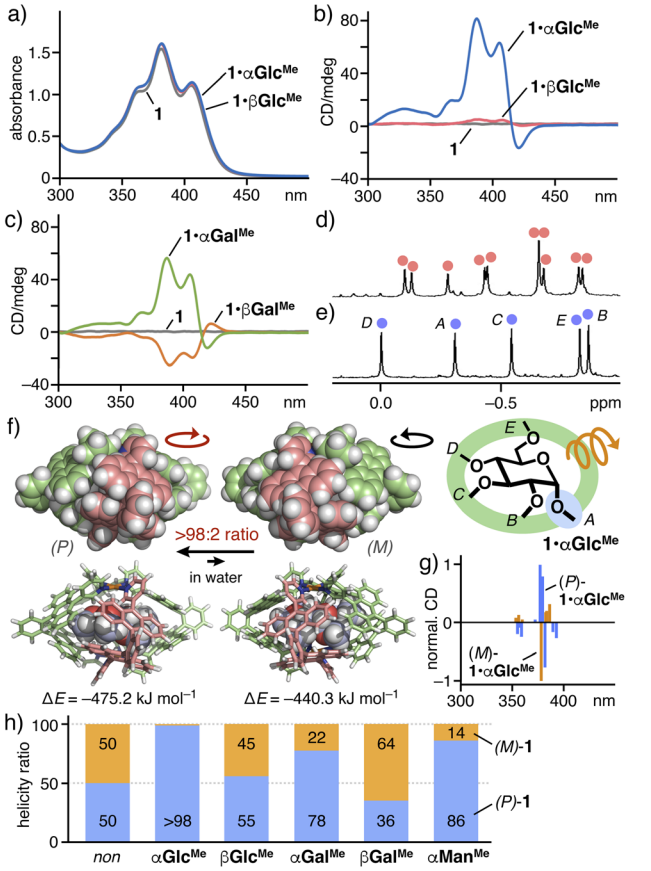

Fig. 6 (a) UV-visible spectra (water, r.t., 0.2 mM based on **1**) of **1**·**αGlc**^{Me}, **1**·**βGlc**^{Me}, and **1**. CD spectra (water, r.t., 0.2 mM based on **1**) of (b) **1**·**αGlc**^{Me}, **1**·**βGlc**^{Me}, and **1**, and (c) **1**·**αGal**^{Me}, **1**·**βGal**^{Me}, and **1**. ^{1}H NMR spectra (500 MHz, D_2O, r.t.) of (d) **1**·**βGlc**^{Me} and (e) **1**·**αGlc**^{Me}. (f) (*P*)/(*M*)-helicity control of capsule **1** upon encapsulation of **αGlc**^{Me} and its optimized structures and energies (R = H for clarity).[19] (g) Theoretical CD spectra of (*P*/*M*)-**1**·**αGlc**^{Me}, calculated by TD-DFT methods (CAM-B3LYP + D3BJ/LanL2DZ (Pd), 6-31G(d,p) (others), PCM (water) level of theory). (h) (*P*)/(*M*)-helicity ratio of **1** with **αGlc**^{Me}, **βGlc**^{Me}, **αGal**^{Me}, **βGal**^{Me}, and **αMan**^{Me} encapsulated in the cavity.

intense positive and negative Cotton effects at 380–420 nm were detected for **1**·**αGal**^{Me} (θ_{max} = +56.4, λ = 386 nm) and **1**·**βGal**^{Me} (θ_{min} = −25.1, λ = 389 nm), respectively (Fig. 6c).

The degree and direction of the capsule helicity of **1**·**αGlc**^{Me} were further estimated by the ^{1}H NMR integrals of the methyl signals, derived from the host–guest complexes, and theoretical CD studies. Whereas the proton spectrum of **1**·**βGlc**^{Me} displayed two sets of the bound guest signals (total 10 CH_3 signals) in a 1 : 1.2 ratio (Fig. 6d),[20] only a single set of those (total 5 CH_3 signals; $H_{A–E}$) appeared in the spectrum of **1**·**αGlc**^{Me} (Fig. 6e), indicating the generation of a single helical structure (>98 : 2 (*P*)/(*M*) ratio based on precision for NMR analysis). The ^{1}H NMR spectra of **1**·**αGal**^{Me}, **1**·**βGal**^{Me}, and **1**·**αMan**^{Me} showed two sets of the bound guest signals (total 10) in 1 : 3.5, 1.8 : 1, and 1 : 6.2 ratios, respectively (Fig. S21–S23†).[16] These results unequivocally revealed the guest-induced formation of **1**·**αGlc**^{Me} as a single-handed helical product to a large extent in water.

The host (*P*)/(*M*)-helicity of **1**·**αGlc**^{Me} was elucidated by the theoretical studies of **1**·**αGlc**^{Me} and empty **1**. The calculated CD

spectrum of (*P*)-**1**·**αGlc^{Me}** obtained by a TD-DFT method displayed intense positive and negative signals at 378–380 and 382 nm, respectively (Fig. 6g). The signal pattern is similar to that of the calculated spectrum of (*P*)-**1** (Fig. S38†).[16] Inverse CD signals were found for (*M*)-**1**·**αGlc^{Me}** and (*M*)-**1** (Fig. 6g and S38†). The theoretical and experimental CD analyses indicated that product **1**·**αGlc^{Me}** adopts a (*P*)/(*M*)-helical structure in >98 : 2 ratio (Fig. 6f and h). The calculated stabilization energies for the formation of the host–guest complexes ($\Delta E(\mathbf{1}\cdot\alpha\mathbf{Glc}^{\mathbf{Me}}) = E(\mathbf{1}\cdot\alpha\mathbf{Glc}^{\mathbf{Me}}) - (E(\mathbf{1}) + E(\alpha\mathbf{Glc}^{\mathbf{Me}}))$) are in the order of (*P*)-**1**·**αGlc^{Me}** < (*M*)-**1**·**αGlc^{Me}** ($\Delta\Delta E(\mathbf{1}\cdot\alpha\mathbf{Glc}^{\mathbf{Me}}) = -34.9$ kJ mol^{-1}; Fig. 6f and Table S1†), supporting the predominant generation (>99 : 1 ratio) of the right-handed twist product. These theoretical studies suggested that the (*P*)-helicity of capsule **1** is also induced by **βGlc^{Me}** (55 : 45 (*P*)/(*M*) ratio based on ^{1}H NMR integrals), **αGal^{Me}** (78 : 22 ratio),[21] and **αMan^{Me}** (86 : 14 ratio), whereas the (*M*)-helicity is induced by **βGal^{Me}** (64 : 36 (*M*)/(*P*) ratio), as major conformations (Fig. 6h).

Conclusions

We have realized the helicity control of a polyaromatic coordination capsule through stereoselective CH–π interactions with permethylated monosaccharides in water. The aqueous polyaromatic capsule with a spheroidal nanocavity was prepared, from metal ions with square-planar coordination geometry and bent bipyridine ligands with cationic groups, as a racemic mixture. Competitive binding studies revealed that the new capsule encapsulates one molecule of permethylated β-glucose with high selectivity (>80 : 20 ratio), from a mixture of α/β-glucoses, due to the equatorial-selective recognition ability. A similar equatorial-selectivity was observed in the binding of β-galactose over α-galactose and β-glucose over β-galactose derivatives by the capsule. The single equatorial/axial substituent configurations on the saccharides could regulate the (*P*)/(*M*)-helicity of the capsule in water. Particularly, an intense Cotton effect was generated upon encapsulation of the α-glucose derivative, unlike the β-glucose, *via* nearly quantitative induction of the (*P*)-helical capsule framework. These results deepen the understanding of helicity control of supramolecular nanostructures through aliphatic CH–π multi-interactions, which will expedite the development of novel chiroptical composites and materials. Moreover, we expect that the combination of the present recognition system with fluorophores holds promise for the creation of highly sensitive receptors toward complex chiral biomolecules in water.

Data availability

The experimental procedures and analytical data are available in the ESI.†

Author contributions

N. K., H. S., T. S., and M. Y. designed the work, carried out research, analysed data, and wrote the paper. M. Y. is the principal investigator. All authors discussed the results and commented on the manuscript.

Conflicts of interest

There are no conflicts to declare.

Acknowledgements

This work was supported by JSPS KAKENHI (Grant No. JP22H00348/JP23K17913) and JST-PRESTO (JPMJPR20A7). Theoretical calculations were performed with the support of Dr Yuya Tanaka (Tokyo Institute of Technology) using computers at the Research Center for Computational Science, Okazaki, Japan (23-IMS-C063). N. K. thanks the JSPS for a Research Fellowship for Young Scientists.

Notes and references

1 E. Yashima, N. Ousaka, D. Taura, K. Shimomura, T. Ikai and K. Maeda, *Chem. Rev.*, 2016, **116**, 13752–13990.

2 (*a*) L.-J. Chen, H.-B. Yang and M. Shionoya, *Chem. Soc. Rev.*, 2017, **46**, 2555–2576; (*b*) M. Pan, K. Wu, J.-H. Zhang and C.-Y. Su, *Coord. Chem. Rev.*, 2019, **378**, 333–349; (*c*) F. Begato, G. Licini and C. Zonta, *Angew. Chem., Int. Ed.*, 2023, **62**, e202311153.

3 Recent reviews: (*a*) C. J. Brown, F. D. Toste, R. G. Bergman and K. N. Raymond, *Chem. Rev.*, 2015, **115**, 3012–3035; (*b*) M. Yoshizawa and L. Catti, *Acc. Chem. Res.*, 2019, **52**, 2392–2404; (*c*) A. B. Grommet, M. Feller and R. Klajn, *Nat. Nanotechnol.*, 2020, **15**, 256–271; (*d*) E. G. Percastegui, T. K. Ronson and J. R. Nitschke, *Chem. Rev.*, 2020, **120**, 13480–13544; (*e*) W. Liu and J. F. Stoddart, *Chem*, 2021, **7**, 919–947; (*f*) L. Escobar and P. Ballester, *Chem. Rev.*, 2021, **121**, 2445–2514; (*g*) H. Takezawa and M. Fujita, *Bull. Chem. Soc. Jpn.*, 2021, **94**, 2351–2369; (*h*) L. Catti, R. Sumida and M. Yoshizawa, *Coord. Chem. Rev.*, 2022, **460**, 214460.

4 (*a*) N. B. Debata, D. Tripathy and D. K. Chand, *Coord. Chem. Rev.*, 2012, **256**, 1831–1945; (*b*) K. Harris, D. Fujita and M. Fujita, *Chem. Commun.*, 2013, **49**, 6703–6712; (*c*) M. Yoshizawa and L. Catti, *Acc. Chem. Res.*, 2019, **52**, 2392–2404; (*d*) S. Pullen, J. Tessarolo and G. H. Clever, *Chem. Sci.*, 2021, **12**, 7269–7293; (*e*) L. K. Moree, L. A. V. Faulkner and J. D. Crowley, *Chem. Soc. Rev.*, 2024, **53**, 25–46; (*f*) E. Benchimol, J. Tessarolo and G. H. Clever, *Nat. Chem.*, 2024, **16**, 13–21.

5 Recent outstanding examples: (*a*) D. Fujita, Y. Ueda, S. Sato, H. Yokoyama, N. Mizuno, T. Kumasaka and M. Fujita, *Chem*, 2016, **1**, 91–101; (*b*) D. Fujita, Y. Ueda, S. Sato, N. Mizuno, T. Kumasaka and M. Fujita, *Nature*, 2016, **540**, 563–566; (*c*) S. Samantray, S. Krishnaswamy and D. K. Chand, *Nat. Commun.*, 2020, **11**, 880; (*d*) K. Wu, E. Benchimol, A. Baksi and G. H. Clever, *Nat. Chem.*, 2024, **16**, 584–591.

6 A. von Zelewsky, *Stereochemistry of Coordination Compounds*, John Wiley & Sons, 1996.

7 Representative M_2L_4 cages as racemic mixtures: (*a*) D. A. McMorran and P. J. Steel, *Angew. Chem., Int. Ed.*,

1998, **37**, 3295–3297; (*b*) J. D. Crowley and E. L. Gavey, *Dalton Trans.*, 2010, **39**, 4035–4037; (*c*) N. Kishi, Z. Li, K. Yoza, M. Akita and M. Yoshizawa, *J. Am. Chem. Soc.*, 2011, **133**, 11438–11441; (*d*) W. M. Bloch, S. Horiuchi, J. J. Holstein, C. Drechsler, A. Wuttke, W. Hiller, R. A. Mata and G. H. Clever, *Chem. Sci.*, 2023, **14**, 1524–1531.

8 (*a*) C. Gütz, R. Hovorka, C. Klein, Q.-Q. Jiang, C. Bannwarth, M. Engeser, C. Schmuck, W. Assenmacher, W. Mader, F. Topić, K. Rissanen, S. Grimme and A. Lützen, *Angew. Chem., Int. Ed.*, 2014, **53**, 1693–1698; (*b*) K. Wu, K. Li, Y. J. Hou, M. Pan, L. Y. Zhang, L. Chen and C. Y. Su, *Nat. Commun.*, 2016, **7**, 10487; (*c*) G. H. Clever, T. R. Schulte and J. J. Holstein, *Angew. Chem., Int. Ed.*, 2019, **58**, 5562–5566; (*d*) X. Tang, H. Jiang, Y. Si, N. Rampal, W. Gong, C. Cheng, X. Kang, D. Fairen-Jimenez, Y. Cui and Y. Liu, *Chem*, 2021, **7**, 2771–2786.

9 Coordination (counter ion)-induced helical cages: I. Regeni, B. Chen, M. Frank, A. Baksi, J. J. Holstein and G. H. Clever, *Angew. Chem., Int. Ed.*, 2021, **60**, 5673–5678.

10 T. K. Lindhorst, *Essentials of Carbohydrate Chemistry and Biochemistry*, John Wiley & Sons, 2007.

11 Permethylated monosaccharide synthesis: T.-R. Li, F. Huck, G. Piccini and K. Tiefenbacher, *Nat. Chem.*, 2022, **14**, 985–995.

12 (*a*) M. Nishio, M. Hirota and Y. Umezawa, *The CH/π Interaction: Evidence, Nature, and Consequences*, Wiley-VCH, 1998; (*b*) H. Takahashi, S. Tsuboyama, Y. Umezawa, K. Honda and M. Nishio, *Tetrahedron*, 2000, **56**, 6185–6191; (*c*) M. Nishio, *Phys. Chem. Chem. Phys.*, 2011, **13**, 13873–13900.

13 (*a*) L. Catti, N. Kishida, T. Kai, M. Akita and M. Yoshizawa, *Nat. Commun.*, 2019, **10**, 1948; (*b*) N. Kishida, K. Matsumoto, Y. Tanaka, M. Akita, H. Sakurai and M. Yoshizawa, *J. Am. Chem. Soc.*, 2020, **142**, 9599–9603; (*c*) N. Kishida, Y. Tanaka and M. Yoshizawa, *Chem. - Eur. J.*, 2022, **28**, e202202075.

14 (*a*) C. Ke, H. Destecroix, M. P. Crump and A. P. Davis, *Nat. Chem.*, 2012, **4**, 718–723; (*b*) R. A. Tromans, T. S. Carter, L. Chabanne, M. P. Crump, H. Li, J. V. Matlock, M. G. Orchard and A. P. Davis, *Nat. Chem.*, 2019, **11**, 52–56; (*c*) W. Liu, Y. Tan, L. O. Jones, B. Song, Q.-H. Guo, L. Zhang, Y. Qiu, Y. Feng, X.-Y. Chen, G. C. Schatz and J. F. Stoddart, *J. Am. Chem. Soc.*, 2021, **143**, 15688–15700.

15 M. Yamashina, M. Akita, T. Hasegawa, S. Hayashi and M. Yoshizawa, *Sci. Adv.*, 2017, **3**, e1701126.

16 See the ESI.†.

17 Dicationic ligand **2** was synthesized from previously reported ligand $\mathbf{3_{MOE}}$ in 27% overall yield (5 steps) using etherification, halogen exchange, and Menschutkin reaction. Capsule **1** formed upon mixing ligand **2** (31 μmol), $PdCl_2(DMSO)_2$ (16 μmol), and $AgNO_3$ (33 μmol) in methanol (0.5 mL) for 3 h at 60 °C.

18 Selective binding of biomolecules: (*a*) M. Yamashina, T. Tsutsui, Y. Sei, M. Akita and M. Yoshizawa, *Sci. Adv.*, 2019, **5**, eaav3179; (*b*) K. Niki, T. Tsutsui, M. Yamashina, M. Akita and M. Yoshizawa, *Angew. Chem., Int. Ed.*, 2020, **59**, 10489–10492; (*c*) R. Sumida, Y. Tanaka, K. Niki, Y. Sei, S. Toyota and M. Yoshizawa, *Chem. Sci.*, 2021, **12**, 9946–9951; (*d*) M. Shuto, R. Sumida, M. Yuasa, T. Sawada and M. Yoshizawa, *JACS Au*, 2023, **3**, 2905–2911; (*e*) R. Sumida, L. Catti and M. Yoshizawa, *ACS Org. Inorg.*, 2024, DOI: 10.1021/acsorginorgau.4c00013.

19 The optimized structures of **1**, $\mathbf{1}\cdot\boldsymbol{\alpha}\mathbf{Glc^{Me}}$, and $\mathbf{1}\cdot\boldsymbol{\beta}\mathbf{Glc^{Me}}$ were obtained by DFT calculations (R = H; CAM-B3LYP+D3BJ/LanL2DZ (Pd), 3-21G (others) level of theory). The CH···π distances were estimated by measuring the distances between the hydrogen atoms of guest CH groups and the ring centres of the host anthracene panels in the optimized structures.

20 No correlation signals between the guests within the (*P*)/(*M*)-helical capsules were observed in the EXSY NMR spectra of $\mathbf{1}\cdot\boldsymbol{\beta}\mathbf{Gal^{Me}}$ in D_2O at room temperature, because of no (*P*)–(*M*) equilibrium (slower than 1.0 s^{-1} inversion rate) under the NMR conditions (mixing time: 1.0, 0.1, and 0.01 s; Fig. S39†).

21 The CD intensity-based (*P*)/(*M*) ratios of $\mathbf{1}\cdot\boldsymbol{\beta}\mathbf{Glc^{Me}}$ and $\mathbf{1}\cdot\boldsymbol{\alpha}\mathbf{Gal^{Me}}$ were estimated to be 52 : 48 and 85 : 15, respectively, which are comparable to their (*P*)/(*M*) ratios based on the ^1H NMR integrals (Fig. 6h).